ACS OMEGA

http://pubs.acs.org/journal/acsodf

Article

First-Principles Investigation of Novel Alkali-Based Lead-Free Halide Perovskites for Advanced Optoelectronic Applications

Banat Gul, Muhammad Salman Khan,* Muhammad Aasim, Ahmad A. lfseisi, Gulzar Khan, and Hijaz Ahmad

Cite This: *ACS Omega* 2023, 8, 32784−32793

Read Online

ACCESS | Metrics & More | Article Recommendations

ABSTRACT: Lead-free halide perovskites are considered promising candidates as visible light absorbers with outstanding optoelectronic properties. In this work, novel kinds of lead-free halide perovskites were studied for their electronic, optical, and thermoelectric properties by employing the most precise and enhanced modified Trans-Blaha Beck-Johnson potential. The estimated band spectra of the studied materials were comparable. The materials are confirmed to have an indirect band gap semiconducting nature due to the existence of energy band gaps. Among the studied materials, $CsSnI_3$ has a smaller band gap, confirming the excitation to be more energy efficient. Examining the predicted density of states and true electronic orbital contributions, we observed a progressive fluctuation along the energy axis was observed. Furthermore, the linear optical properties are calculated and studied in terms of possible optoelectronic applications. The absorption in $KSnI_3$ was greater compared to the other two materials. The studied materials could be used for antireflecting coatings against UV radiation, owing to the prominent peaks in their reflectivity spectra. The Seebeck coefficient and electrical properties, as well as the positive value of R_H all pointed to a p-type nature in these materials. From the anticipated thermoelectric properties, the materials also appear to be suitable for application in thermoelectric devices.

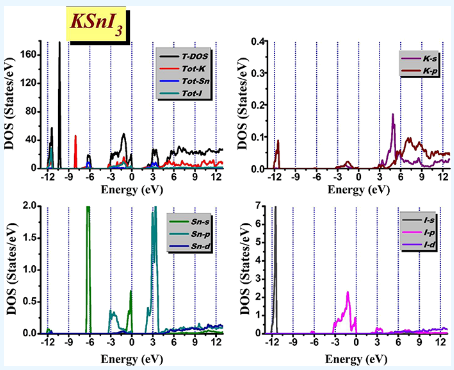

1. INTRODUCTION

The search for novel material systems with specialized enhanced functioning is extremely essential for the advancement of science. The materials' extremely strong bonding exhibits ironic physics that offers some astonishing possibilities for their electronic, optical, and thermoelectric behavior. Advanced optoelectronic equipment has a growing demand for innovative semiconducting materials with suitable properties, which is being met.[1] Research into new perovskites is presently concentrated in a variety of sectors for their potential use in solar cells and other devices, which have caught the interest of scientists. Due to their ability to absorb light, these materials are also used in light sensors.[2−456] They have also attracted a lot of attention due to their efficient light accumulation qualities and contributions as postproduction photovoltaics. In addition to having high peak absorption capacities, the various halide perovskite models have direct-type band structures in the visible and ultraviolet range, revealing the potential of these combinations for use in solar cell implementations. Additionally, similar to these perovskite mixes, their use in memory devices, superconductors, dielectrics, laser diodes, and light-emitting diodes (LEDs) were also found.[7] These halide-type Perovskites are employed in the production of LEDs and light-pumped luminous bodies as a luminescent material.[8,9] First, the pure inorganic perovskites $CsPbX_3$, which has a structure comparable to $CaTiO_3$ (testified as the first phase of a perovskites compound), was examined by MØLLER et al.[44] However, the alteration efficiency is shown to be very low.[10] The exchange of cesium (Cs) to methylammonium (MA) and formamidine (FA), but these compounds have additional concerns with durability, brings out the band gap in a blue shift via 1.48 eV in $CsPbX_3$ in advance.[11−13]

A practical theoretical impression that precisely determined the optical and electronic behavior of these perovskite components should be established to obtain the desired outcome. When compared with similar inorganic perovskite halide materials, the $CsPbI_3$ demonstrates higher photovoltaic performance.[30,31] Even yet, the $CsPbI_3$ undergoes a non-perovskite transformation at ambient temperature that results in a structure that has a band gap of 2.83 eV and a negligible

Received: May 30, 2023
Accepted: August 11, 2023
Published: August 25, 2023

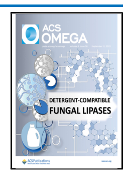

ACS Publications

https://doi.org/10.1021/acsomega.3c03756
ACS Omega 2023, 8, 32784−32793

photovoltaic effect. As compared to earlier organic and inorganic hybrid perovskites, switching Rb to Cs is predicted to boost the device's reliability.[32−34] This material is preferable to other solid-state systems in electrolytes having TiO_2 for dye-sensitized Gratzel solar cell materials[15] because it has high mobility power in addition to $CsSnI_3$.[14] The well-organized solar radiation absorption constituents in this kind of perovskite comprise mixed halide perovskites made of cesium (Cs) and tin (Sn).[16,17] Contrary to most semiconducting materials, the intriguing features of $CsSnI_3$ are linear with a considerable rise in bandgap energy (E_g) along with an increasing temperature.[35] $CsSnI_3$ has been used in innovative devices for lead-free light absorbers and substantial optical qualities despite its usage as hole-transporting material in photovoltaics.[36−38] This is due to the consequent surge in action carried by the perovskites solar cell.[39] Like many perovskites,[40] $CsSnI_3$ displays a complex phase diagram that is determined by small energy rotation and tilting of SnI_6 octahedral.[41] According to a study by Saliba et al., adding Cs^{1+} further stabilized these perovskite structures and improved the PCE and reproducibility of solar cell manufacturing.[18] The same team would be compelled by further optimization to incorporate RbI into the perovskite pioneer solution.[19] Since the presence of lead (Pb) in lead-based perovskites is one of their main limitations, our investigated halide perovskites are lead-free.

The EU's Constraints of Hazardous Contents regulation prohibits the utilization of lead (Pb) in all electronic and electrical devices because of its toxic effects. As a result, substitutes to lead as metallic cations in the perovskite photoabsorber are increasing and gaining importance.[20] In the field of solar cell technology, $RbSnI_3$, $KSnI_3$, and $CsSnI_3$ could be emerging substitutes for conventional lead-based perovskites. Due to their comparable photovoltaic performance and potential to address the stability and toxicity issues with lead-based perovskites, these materials have drawn a lot of interest. Similar in crystal structure and displaying excellent optical and electronic characteristics, $RbSnI_3$, $KSnI_3$, and $CsSnI_3$ have bandgaps that are good for effective solar absorption and charge transfer. They also have substantial carrier lifetimes and strong carrier mobilities, which point to their potential for effective charge separation and collection. Before these intriguing alternatives can take the place of conventional lead-based perovskites commercially, more investigation and optimization are required to improve their stability and long-term performance. We chose to investigate these lead-free halide perovskites and inspect their composition and optical, electronic, and thermoelectric characteristics because of their stability, minimal toxicity, and small value of cost. We chose to investigate these lead-free halide perovskites and inspect their composition, and optical, electronic, and thermoelectric characteristics because of their stability, minimal toxicity, and small value of cost. Here, in the present work, a new type of orthorhombic $ASnI_3$ (A = K, Rb, and Cs) perovskites are being examined. Results of the calculations we performed are presented in the second section of our comprehensive review, and the electronic structure, optoelectronic, and transport outcomes are examined in the third section. We emphasize the utmost important findings from the present research in the final section.

2. COMPUTATIONAL DETAILS

The BoltzTrap tool and the Wien2k software, respectively, were used to analyze the structural, optical, electrical, and transport properties of these materials, both utilizing the state-of-the-art full potential linearized augmented plane wave technique.[21] The modified Trans-Blaha Beck-Johnson potential (TB-mBJ) and GGA provide examples of the fundamental characteristics of a structure.[22] Becke and Johnson created and identified a distinct kind of ex-correlation. This technique is used to obtain the exchange-correlation effects.[23] The potential is stated as follows, and the reference includes additional details:[24]

$$v_{x,\sigma}^{\mathrm{MBJ}}(r) = c v_{x,\sigma}^{\mathrm{BR}}(r) + (3c-2)\frac{1}{\pi}\sqrt{\frac{5}{12}}\sqrt{\frac{2t_\sigma(r)}{\rho_\sigma(r)}} \quad (1)$$

The orthorhombic structure of our examined halide-type materials is depicted in Figure 1 together with the computed

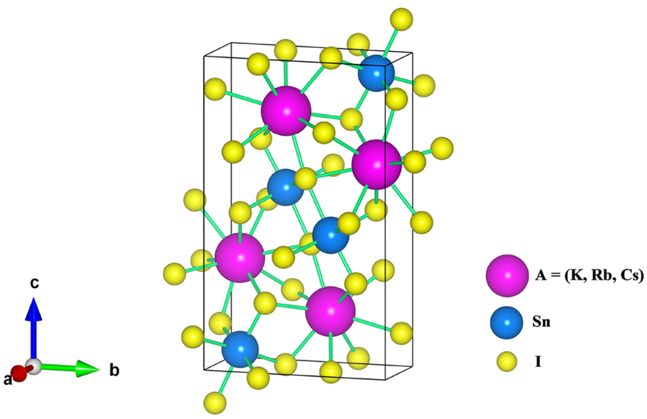

Figure 1. Crystal structure with Vesta for the studied materials.

unit cell structure. The BoltzTrap method was additionally used to compute the thermoelectric characteristics.[43] Onsager equations and the Boltzmann Transport Theory are used to get the significant thermoelectric properties:

$$\mathbf{J} = \sigma \mathbf{E}_0 - \sigma S \nabla T \quad (2)$$

$$\mathbf{J} = \sigma S T \mathbf{E}_0 - \kappa \nabla T \quad (3)$$

The variables that replicate the gradient of temperature, electrical conductivity, Seebeck coefficient, and external electric field are ∇T, σ, S, and $\mathbf{E}_0$ respectively. Thus, the symbol for thermal conductivity was obtained by applying the Wiedmann−Franz law to the electric conductivity.

3. RESULTS AND DISCUSSION

3.1. Electronic Properties.

3.1.1. Electronic Band Structures. We investigated orthorhombic, "*P*" type, computed unit cells for $ASnI_3$ (A = K, Rb, and Cs) with space group *P*222 and group number 1. For the halide perovskites $KSnI_3$, $RbSnI_3$, and $CsSnI_3$, the computed unit cell volumes are 862.74, 861.45, and 860.96 Å^3, respectively. The calculated fundamental lattice parameters for $KSnI_3$ were 4.78 10.38, and 17.34 Å, for $RbSnI_3$, were 4.62 12.18, and 18.13, 12.18, 18.13 Å and for $CsSnI_3$ the values were 4.89 11.84, and 18.56 Å, respectively (see Table 1) along with their respective lattice angles α, β, and γ all equals to 90° respectively. This demonstrated that our projected lattice constants for $CsSnI_3$

https://doi.org/10.1021/acsomega.3c03756
ACS Omega 2023, 8, 32784−32793

Table 1. Computed Atomic Positions, Lattice Constants, Unit Cell Volume, Formation Energy (E_{form}), and Bulk Modulus (B)

	WC-GGA								
atoms	x	y	z	a (Å)	b (Å)	c (Å)	V_0 (Å)	E_{form} (eV/f.u.)	B (GPa)
					$KSnI_3$ (P222)				
K	0.419	0.250	0.172	4.78	10.38	17.34	862.74	−1.13	73.16
Sn	0.158	0.250	0.503	4.89[35]	11.36[35]	18.24[35]			
I	0.474	0.750	0.617						
					$RbSnI_3$ (P222)				
Rb	0.837	0.750	0.060	4.62	12.18	18.13	861.45	−1.47	76.01
Sn	0.300	0.250	0.788	4.13[36]	10.14[36]	17.17[36]			
I	0.837	0.750	0.495						
					$CsSnI_3$ (P222)				
Cs	0.825	0.750	0.059	4.89	11.84	18.56	860.96	−1.68	77.14
Sn	0.350	0.250	0.875	5.17[37]	11.23[37]	17.01[37]			
I	0.976	0.750	0.474						

and those calculated by Aggarwal et al.[26] matched very well. The WC-GGA was used to determine the optimized locations for each atom, and the results are revealed in Table 1. Similarly, the formation energy is also calculated and is presented in Table 1 in order to estimate the stability of their thermodynamic nature. Each of the structural phases of the materials under study rests significantly lesser as compared to the corresponding elemental hull, with a limit of −1.31 to −3.00 eV/f.u. These formation energies suggest that the Sn−I bonds have an extremely strong connection and an ionic nature. As seen in Figure 2a−f, the band profiles we calculated for the three materials are comparable. Additionally, each of these three halide perovskites has a significant gap between its valence band (VB), which is a band of connected electrons, and its conduction band (CB), which is a band of free electrons, according to the determined band structure visibility for each of these materials, demonstrating that each of these three substances is a semiconductor.[27] Our estimated gap values for the $KSnI_3$, $RbSnI_3$, and $CsSnI_3$ materials using TB-mBJ are predicted to be 2.31, 2.42, and 0.58 eV, respectively. These materials exhibit an indirect band gap, which is supported by the fact that the highest point of the confined electron band (VB) and the lowest elevation of the free electron band (CB) are not situated at the same high symmetric Γ point in the predicted band features. Then, using the mBJ approach, we find that the $CsSnI_3$ has a bandgap value of 0.58 eV, which makes it slightly different as compared to the other materials. Similarly, to the above, a lower bandgap value for $CsSnI_3$ compared to the other two halide perovskite materials implies a lower energy level for electron excitation. Similar band structures were noticed from the estimated band profiles of these materials shown in Figure 2a−f. The topmost region of the VB closer to the Fermi level was highly impacted by I-p states, with a few minor contributions by the Sn-s and Sn-p states, according to the density of state data. On the other hand, these materials' equivalent Sn-s orbitals are what give rise to the lowermost bands of the VB. The Sn-p orbitals also contributed to the development of the CBs in these materials. The alkali ions in these three compounds seem to have created ionic connections with other lattice atoms. Therefore, it is most likely that the σ_{p-p} interaction is caused by the highest occupying molecular orbitals, which are found between I-p_z and Sn-p_z at energies up to 0.0 eV within the VB. The CASTEP package,[43] which also operates within the framework of density functional theory, is used for calculating graphs of the phonon dispersions for the materials under study in Figure 3a−c. The phonon dispersion calculations predicted and confirmed the studied materials' stable nature. The results of our calculations conclusively show that the absence of negative frequencies proved that the material systems that we examined have stable structures.

3.1.2. Density of States. Figure 4 displays the density of states for the examined halide perovskites. Here, we used two distinct features: the orbital and overall contributions to demonstrate the computed density of state plots. To further comprehend by using the most precise approximation, we calculated the total plus the partial density of states for these three halide perovskites $ASnI_3$ (A = K, Rb, and Cs). The dotted lines in these revealed plots stand for the Fermi level. These plots also confirm the semiconducting nature of these compounds. In the case of $KSnI_3$, we found that the K atoms' VB, from 10.0 eV and close to the Fermi level, contributes significantly to the observed peaks and evaluates a relative influence of multiple electronic (s, p, and d) states in these materials. Additionally, it can be demonstrated that the K-s orbital contributes more to the CB at about 5.0 eV than the K-s orbital does to the VB at −12.0 eV by looking at the partial density of states of specific elements, such as potassium. The Sn-p and Sn-d contributions to the VB are both insignificant, similar to Sn-s, whereas the contribution of Sn-s is large at about −6.0 eV. Furthermore, at 3.0 eV, Sn-p contributes most to the CB. We examined the partial density of $KSnI_3$ with the conclusion that the I-s are responsible for the first peak at around −12.0 eV in the VB. We also deduced from $RbSnI_3$ plots that Rubidium atoms have a leading role near the Fermi level in the VB up to 10.0 eV. While investigating the partial densities of states of the Rubidium-based system, the p-orbital of Rb at approximately −10.0 eV is responsible for the major influence in the VB, while the contribution of the Rb-d orbital is only marginally evident in the CB and the rest are insignificant minorities. The majority of the VB contributions in these systems are found to be influenced by the Sn-s, with the Sn-p and Sn-d making up the least percentage of the total. The Sn-p makes the major contributions in the CB at about 3.0 eV, proving that the Sn contribution in $KSnI_3$ is equivalent. The initial peak at the end of the $RbSnI_3$ system is created by I-s at around −12 eV in the VB, according to our investigation. The I-p interaction plays an important role and is quite close to the Fermi level at about −3.0 eV. A few small peaks at around −3.0 eV and near the Fermi level were observed, and the combined contribution of Cs to the total density of states in the $CsSnI_3$ combination was first noticed at −9.0 eV. The Cs-p

https://doi.org/10.1021/acsomega.3c03756
ACS Omega 2023, 8, 32784−32793

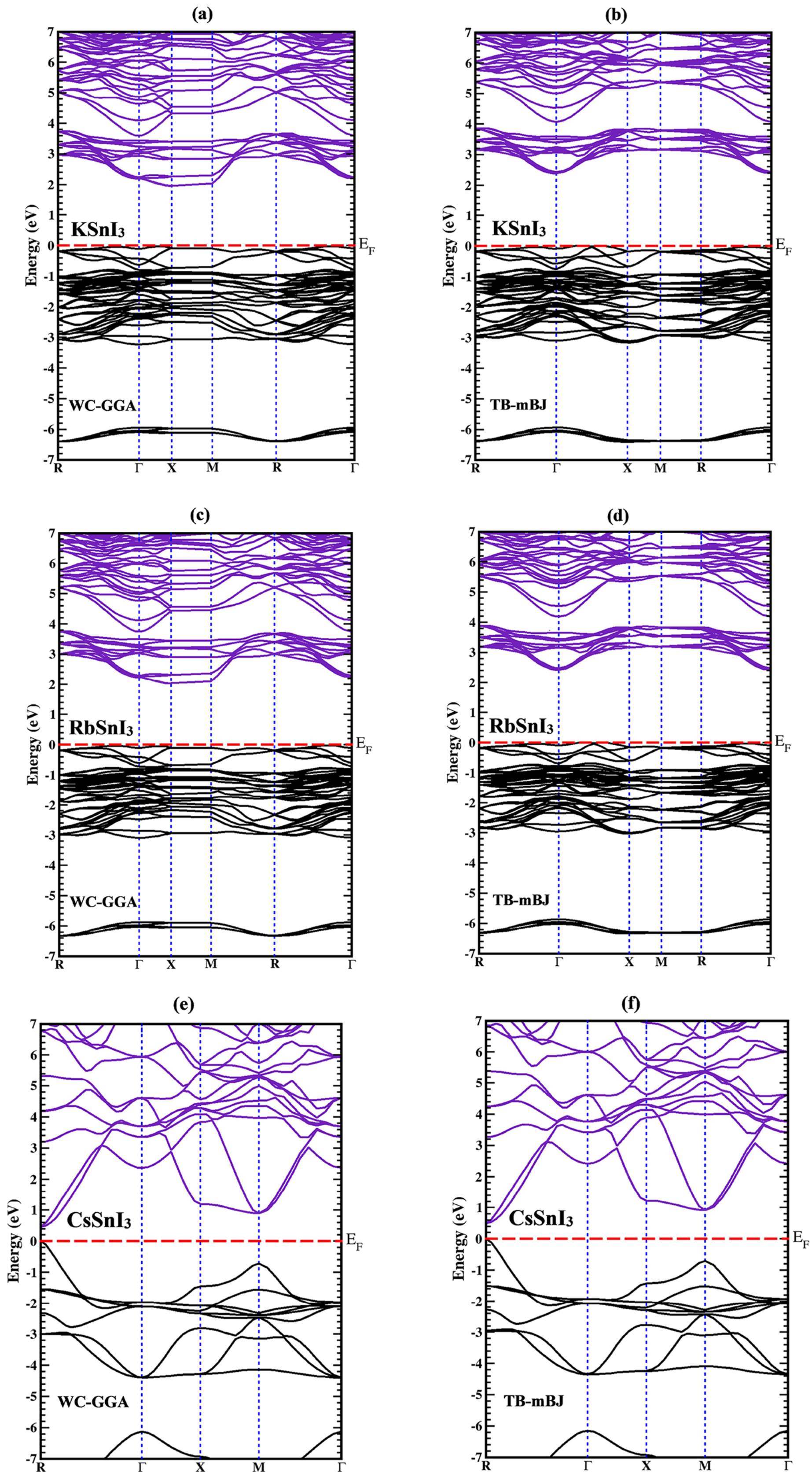

Figure 2. Band structure profiles for (a, b) $KSnI_3$, (c, d) $RbSnI_3$, and (e, f) $CsSnI_3$ with both WC-GGA and TB-mBJ potentials.

orbital of the element cesium (Cs) causes a significant peak at −9.0 eV in the VB, though the other orbitals' contributions to the conduction and VBs are minimal. For this case, the Sn-s orbital's contribution is larger in the VB between −9.0 and −6.0 eV. The Sn-p states, which were wide and elevated at 4.0 and 0.5 eV, close to the Fermi level, are what contribute most

https://doi.org/10.1021/acsomega.3c03756
ACS Omega 2023, 8, 32784−32793

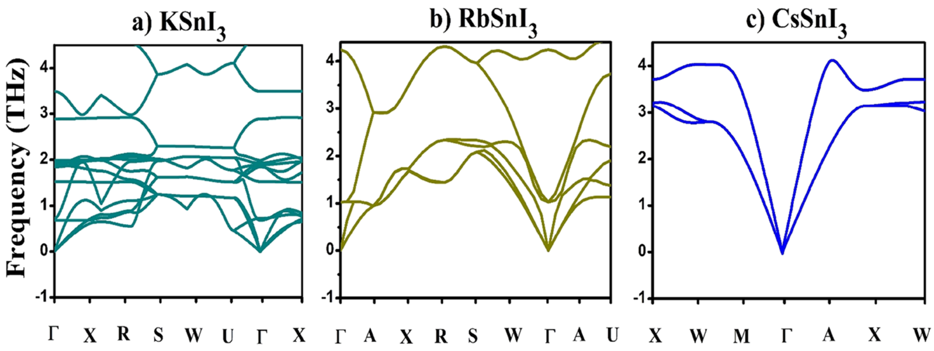

Figure 3. Phonon dispersion plots for (a) $KSnI_3$, (b) $RbSnI_3$, and (c) $CsSnI_3$.

to the CB. The contribution of I-s and I-p is maximum in the VB of iodine at −12.0 and −2.0 eV, respectively. Additionally, there is just a small amount of I-p at 4.0 eV in the CB and no significant contributions.

3.2. Optical Properties. It is essential to examine a material's responses in the infrared, visible, and ultraviolet spectra for a better understanding of its optoelectronic capabilities.[25] Some of the significant optical properties. The supplied perovskites' polarizability is made clear by the real component of the dielectric function, $\varepsilon_1(\omega)$, displayed in Figure 5a, and computed absorptive behavior is indicated by the $\varepsilon_2(\omega)$, which is the imaginary component. A rise in performance was seen in these materials for narrower bandgap values. According to the formula $\varepsilon_1(0) \approx 1+(h\omega_p/E_g)^2$, these static values correlate to the bandgap, meaning that a smaller E_g will result in a larger $\varepsilon_1(0)$. This link was accurately captured by Penn's model.[42] According to Figure 5a, the detected static values $\varepsilon_1(0)$ for the three materials (Table 2) are 5.6, 5.4, and 7.9, respectively. Our estimated $\varepsilon_1(0)$ for $RbSnI_3$ was found to agree with the value reported in the literature, which was estimated to be around 5.45 by Nyayban et al.[33] According to Figure 5b, $KSnI_3$, $RbSnI_3$, and $CsSnI_3$ have high peak points in the imaginary component at about 3.0, 3.0, and 1.5 eV, respectively. Results demonstrate that, when compared to the other two compounds, $KSnI_3$ has the highest polarizability at around 3.0 eV, whose value is around 10.2. With a first high peak of 9.9 at 3.0 eV, it exhibits performance that is basically identical to that of the $RbSnI_3$. We discovered a peak of about 9 at 1.0 eV for the $CsSnI_3$ material, which is slightly larger than the other two materials. We notice that the polarizability of the $KSnI_3$ and $RbSnI_3$ moves to the region's opposite side and then increases for energy values around 5.0 eV. After some time, it starts to drop at 7.5 eV once more before continuing to move in the direction of the negative zone. In contrast, the high peak of $CsSnI_3$ is around 0.9, and after that, the value remains to fall beneath 8.20 eV. In fact, the imaginary component of the observed dielectric function shows how electromagnetic radiation interacts with the materials and how they absorb energy.[28] The absorptive reaction of these three halide perovskites is revealed by the imaginary portion of the function and is directly assumed along the electronic band arrangement.[29]

The initial peak for the imaginary component for $KSnI_3$, $RbSnI_3$, and $CsSnI_3$ appears to be at about 4.0, 4.1, and 2.5 eV respectively. The peaks in the fictitious portions were probably created by the development of allowed carriers from the restricted phase to the free phase. From 0.5 to 6.5 eV, the maximum value of $CsSnI_3$ is seen to rise quickly. As a result, research demonstrated that the absorption of substances starts to occur in the visible and UV bands when the radiation intensity reaches high levels. All of the $KSnI_3$, $RbSnI_3$, and $CsSnI_3$ materials had absorption coefficients that start to rise over 2.0 2.0, and 0.9 eV, respectively, as revealed in Figure 5c. These materials can be employed as possible candidates for optoelectronic device applications that operate in the UV spectrum because of their sharp cutoff response, which occurs mostly in the regions with the highest energy. To sum up the issue, we can say that these sources are suitable for both LEDs and lasers because we purchased them in the IR region and because they will absorb lighter than any other substance. For $KSnI_3$, $RbSnI_3$, and $CsSnI_3$, respectively, the primary peaks of the energy loss function curve are seen in Figure 5d to occur at 13.0, 13.2, and 12.0 eV. Plasma resonance that takes place at the plasma frequency is specified by the $L(\omega)$, which is a distinctive property. Furthermore, the crucial feature of these traits that are connected to the plasma resonance is also very significant. Comparing $CsSnI_3$, a mixed compound containing cadmium, to the other two materials, we see some high-curve peaks.

The static reflectivity $R(\omega)$ for these three halide perovskites is shown in Figure 6a, with values for $KSnI_3$, $RbSnI_3$, and $CsSnI_3$ being about 0.16, 0.17, and 0.23, respectively (see Table 2). Our predicted $R(0)$ value for $RbSnI_3$ is reasonably close to Nyayban et al.'s estimate of 0.163.[33] For $KSnI_3$, $RbSnI_3$, and $CsSnI_3$, the highest reflectivity $R(\omega)$ values are 0.59, 0.59, and 0.52 correspondingly. These high reflectivity $R(\omega)$ values show a better indication for their usage as a coating material that reduces reflection. Figure 6b shows the plots for $n(\omega)$. For $KSnI_3$, $RbSnI_3$, and $CsSnI_3$, we observed static values of 2.26, 2.27, and 2.76, respectively (Table 2). The extension coefficients of the two materials, $KSnI_3$ and $RbSnI_3$, as shown in Figure 6c, are relatively small at first, but they start to increase at 1.9 eV and peak at 4.5 eV, with values of 2.0 and 1.7, respectively. However, if we observe $CsSnI_3$, the value immediately increases from the initial value of 0.2 eV, which then approaches a high value of around 1.48 at 2.8 eV.

3.3. Thermoelectric Properties. For use in computing cooling processes, tiny detector components, thermoelectric refrigeration, and other applications, thermoelectric materials have been the subject of intense research during the past few decades. A heat gradient is created by the movement of charge to transfer energy, which in turn creates a potential difference and the thermoelectric effect. High electrical conductivity, lower thermal conductivity, and larger Seebeck values all contribute to enhanced thermoelectric efficiency. The relaxation time is important because it affects how the

https://doi.org/10.1021/acsomega.3c03756
ACS Omega 2023, 8, 32784−32793

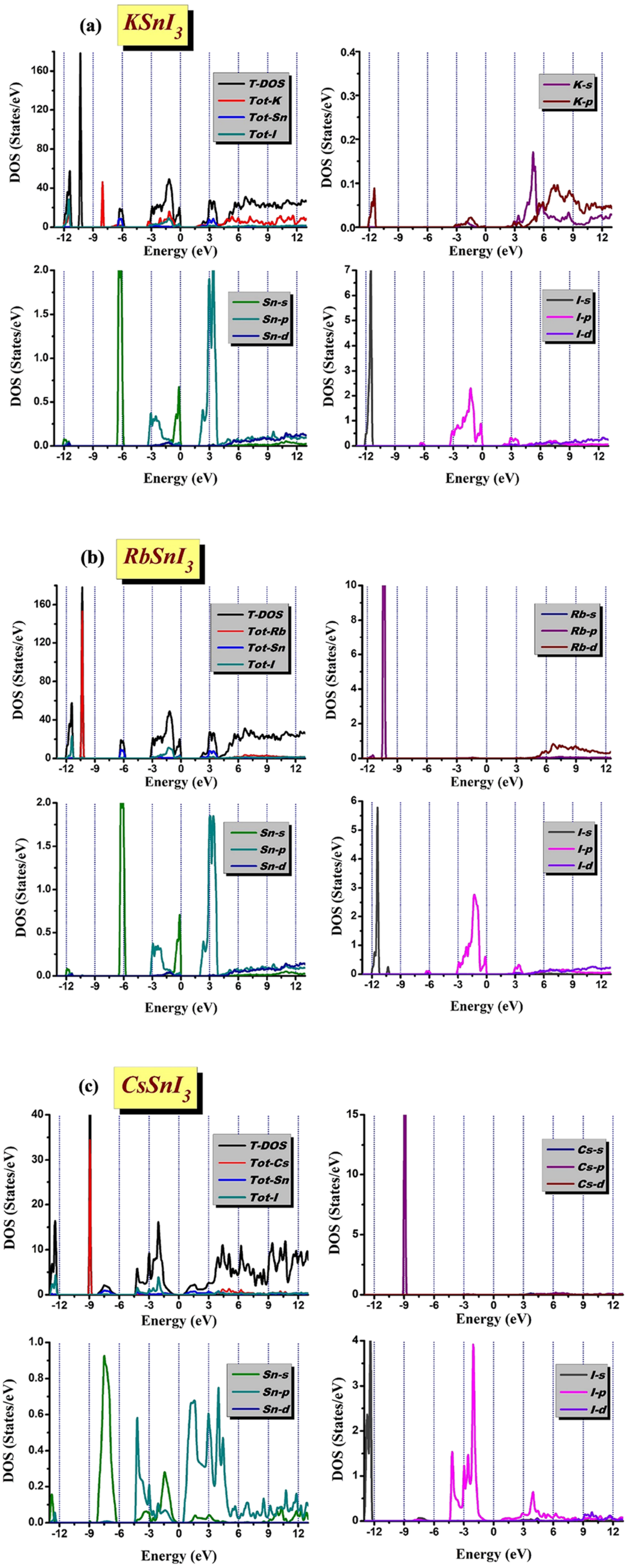

Figure 4. Projected density of states for (a) $KSnI_3$, (b) $RbSnI_3$, and (c) $CsSnI_3$.

semiclassical Boltzmann transport theory's relaxation time approximation calculates the electronic transport coefficient of the TE material. Numerous scattering processes, such as magnetic scattering, electron–electron interactions, electron–phonon interactions, defects, impurity scattering, etc., frequently influence the relaxation time. As a result, selecting a time to rest is frequently challenging. Typically, calculations of thermal and electrical conductivity are based on the presumption that the relaxation time is independent of energy and is calculated equal to 7.3×10^{15} (s). When comparing $KSnI_3$, $RbSnI_3$, and $CsSnI_3$, which have poor thermal conductivities, in Figure 7a, the thermoelectric performance is determined and plotted versus temperature. The slope of $CsSnI_3$ is significantly larger compared to that of $KSnI_3$, and $RbSnI_3$ due to the increased electronic energy in the material. The Seebeck coefficient, which shows two zones, one above and the other below zero, was calculated. When the value is more than zero, holes seem to make up the majority of charge carriers, but when the value is lower than zero, electrons do. The Seebeck coefficient of $KSnI_3$ is zero at ambient temperature (300 K), while that of $RbSnI_3$ is approximately 22 μV/K, and for $CsSnI_3$ is 35 μV/K. As a result, $CsSnI_3$ material is considered to be of more interest in these materials. Figure 7b, which depicts the estimated Seebeck coefficient, shows that for $KSnI_3$, $RbSnI_3$ declines with rising temperature. At ambient temperature, $RbSnI_3$ has a greater value for $KSnI_3$ than $CsSnI_3$. The value begins to rise with temperature after increasing the temperature.

Utilizing specific heat capacity, a crucial aspect was to see lattice oscillations from a different perception. Figure 7c, which shows the studied specific heat capacity (C_v), shows that materials with higher melting points, including $KSnI_3$, $RbSnI_3$, and $CsSnI_3$, have greater C_v values than materials with lower melting points. We examined particular heat capacities that were solely reliant on electrical inputs. At temperatures of about 100 K, the specific heat capacities were 1.1, 1.0, and 0.75 J mol K^{-1}, respectively. The maximal C_v values for $KSnI_3$, $RbSnI_3$, and $CsSnI_3$ at 850 K are roughly 11.1, 10.28, and 6.90 J mol K^{-1}, respectively. Therefore, materials that have lower specific heat capacities are more capable of recognizing temperature change. Their application is justified by the fact that they are unlikely to become too heated. However, materials with a high specific heat capacity proved to be suitable for making oven covers and insulating materials. According to Figure 7d, the power factor of $CsSnI_3$ at 300 K is zero, while it is 0.38 for $RbSnI_3$ and 0.2 for $KSnI_3$. The power factor (PF) peaks for $KSnI_3$, $RbSnI_3$, and $CsSnI_3$ appear to exist at 200 K, but the peaks for $CsSnI_3$ degrade and become lower at 300 K.

In Figure 8a, the ZT for these investigated materials is depicted as rising with temperature. Similarly, due to the fact that for $KSnI_3$ ZT was about 0.021 at normal temperature, it

Table 2. Zero Frequency Limits for the Static Dielectric Constant $\varepsilon_1(0)$, the Reflectivity $R(0)$, and the Refractive Index $n(0)$

	$KSnI_3$	$RbSnI_3$	$CsSnI_3$	
$\varepsilon_1(0)$	5.6	5.4	7.9	present work
	5.8[35]	5.66[35]		others' work
	5.43[36]			
$R(0)$	0.16	0.17	0.23	present work
	0.18[35]	0.16[33]		others' work
	0.21[36]			
$n(0)$	2.26	2.27	2.76	present work
	2.14[35]	2.16[35]		others' work
	2.36[36]			

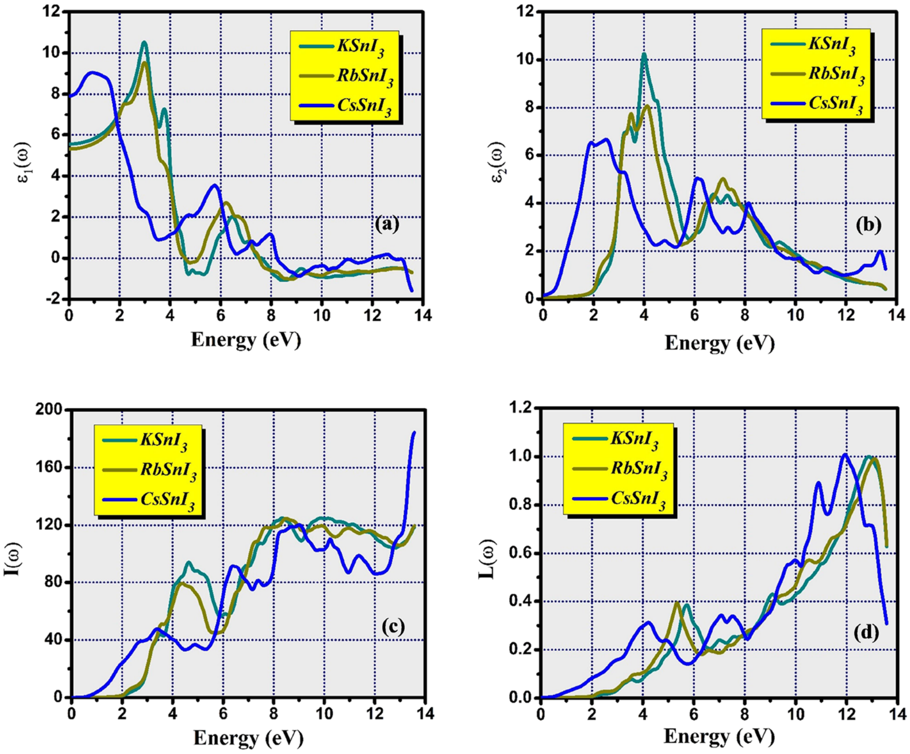

Figure 5. Frequency-dependent (a) real part, (b) imaginary part of the dielectric function, (c) absorption coefficient, and (d) energy loss function.

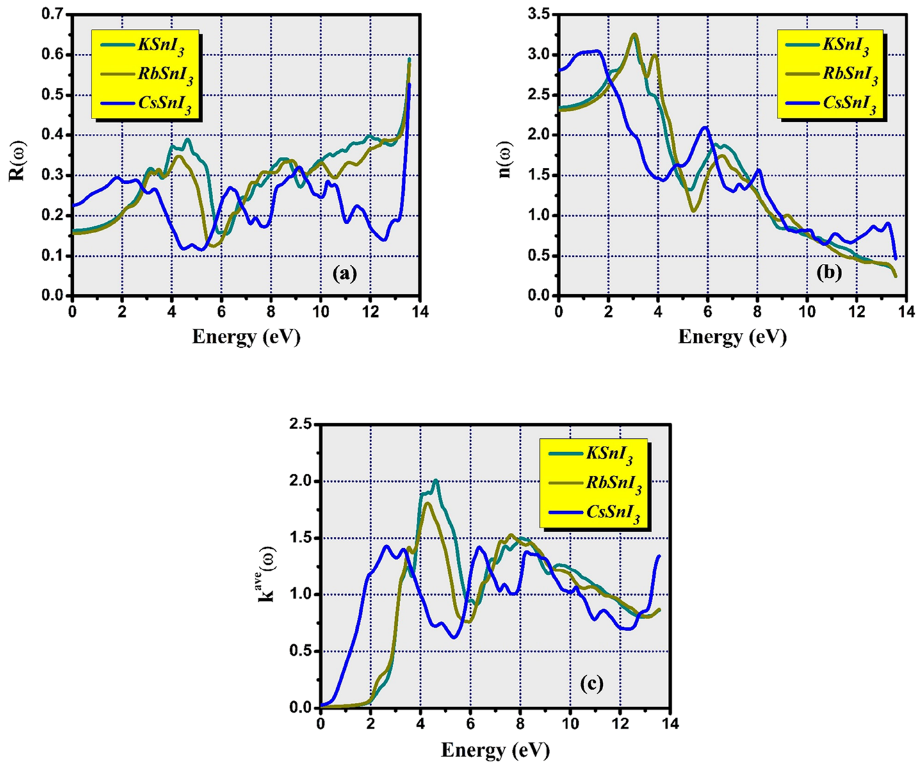

Figure 6. Frequency-dependent (a) reflectivity, (b) refractive index, and (c) extinction coefficient.

drops and reaches about 0.005 at 800 K, and similar to for $CsSnI_3$ material *ZT* was zero at the same normal temperature which then rises and reaches a high level of about 0.01 at temperatures of around 800 K; the highest possible value for $RbSnI_3$ is about 0.05 in comparison to both of the other two materials. Lower Seebeck coefficients and thermal conductivities better than those of $RbSnI_3$ allow $KSnI_3$ and $CsSnI_3$ to have lower *ZT* profiles. The *ZT* of $RbSnI_3$ rises to 0.052 between (200−300) K and thereafter falls. The *ZT* for $CsSnI_3$ halide perovskite, on the other hand, is about 0.015 at 100 K and declines at 300 K. Additionally, the *ZT* for $KSnI_3$ is 0.022 at 300 K, which is the peak value. The Curie−Weiss constant

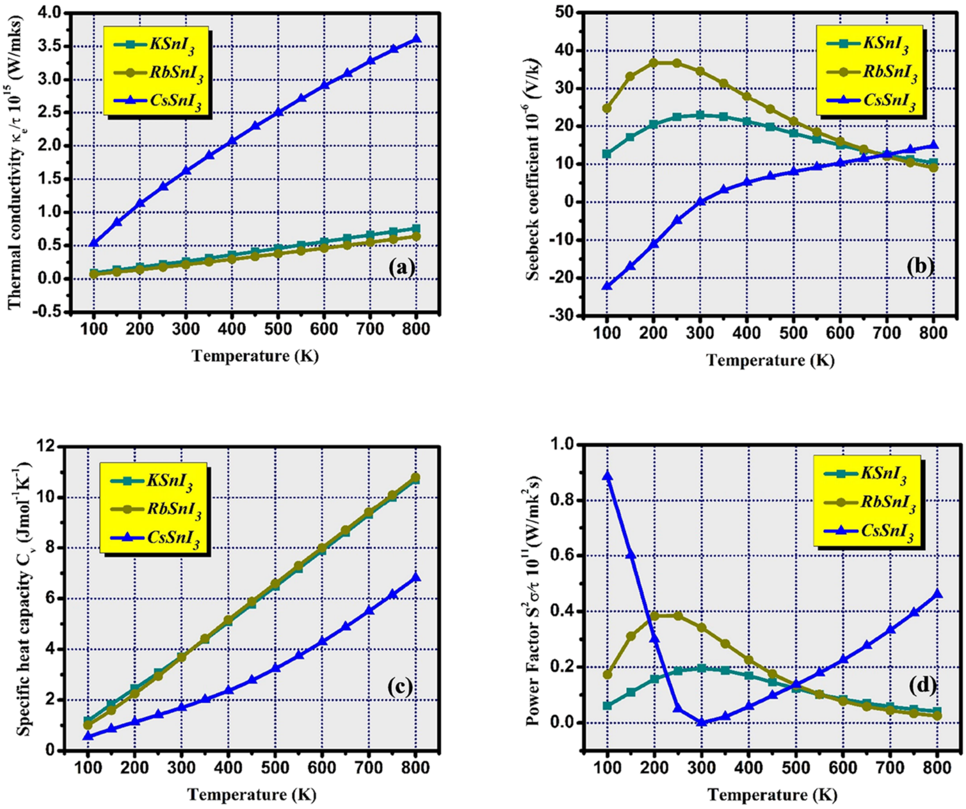

Figure 7. Temperature-dependent (a) thermal conductivity, (b) Seebeck coefficient, (c) specific heat capacity, and (d) power factor.

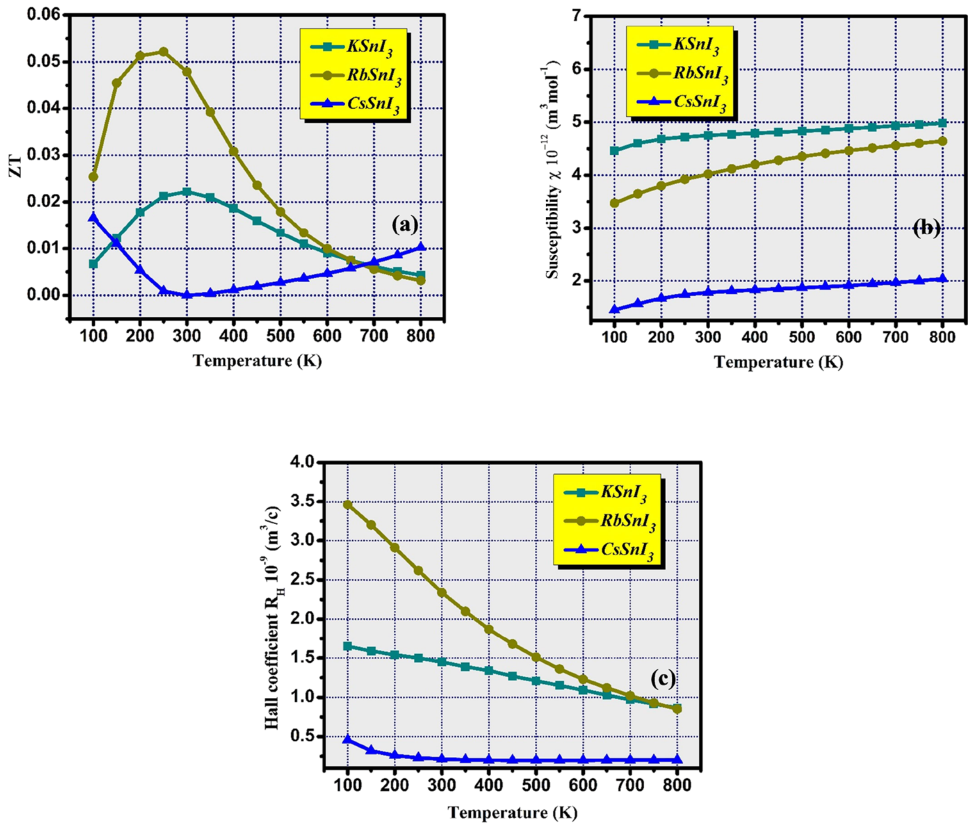

Figure 8. Temperature-dependent (a) figure of merit, (b) susceptibility, and (c) Hall coefficient.

(T), which is positive for the materials $KSnI_3$, $RbSnI_3$, and $CsSnI_3$, can be determined by analyzing the susceptibility, as shown in Figure 8b. The susceptibility values for $KSnI_3$, $RbSnI_3$, and $CsSnI_3$ are 4.5×10^{-12}, 3.5×10^{-12}, and $1.0 \times$

https://doi.org/10.1021/acsomega.3c03756
ACS Omega 2023, 8, 32784−32793

10^{-12} (m^3 mol^{-1}) at about 100 K, respectively, and they increase to 5.0×10^{-12}, 4.5×10^{-12}, and 2.0×10^{-12} (m^3 mol^{-1}) at 800 K, respectively. The kind, quantity, and characteristics of the charge carriers that make up the current value have an impact on the Hall coefficient, as can be seen in Figure 8c. The charge carrier concentration and mobility are responsible for the coefficient R_H's constant positive relationship with temperature. These materials are p-type, as shown by the Seebeck coefficient, and their positive R_H values are compatible with their electrical characteristics. Initially high at 100 K, the R_H for $KSnI_3$, $RbSnI_3$, and $CsSnI_3$ then swiftly decreases.

4. CONCLUSIONS

The novel halide perovskite $ASnI_3$ (A = K, Rb, and Cs) electronic, optical, and thermoelectric properties have been determined by employing density functional theory calculations with a TB-mBJ technique. The VB maximum and CB minimum do not lie at their Γ point, which is clearly visible in the band profiles and indicates that the materials have an indirect band gap. Our calculated band gap values 2.20 eV for $KSnI_3$, and 0.58 eV for $CsSnI_3$ are not located at the same Γ point, nor are the VB maximum and CB minimum. $CsSnI_3$ would require less energy for excitation since its gap value is lower than that of the other two halide perovskite materials. The imaginary component $\varepsilon_2(\omega)$ reveals absorptive behavior in the situations of $KSnI_3$, $RbSnI_3$, and $CsSnI_3$ at 3.0, 3.0, and 1.5 eV, respectively, and has a high peak, showing that the polarizability of $KSnI_3$ was much greater than that of the other compounds. The compound $KSnI_3$ has the largest absorption capacity for electromagnetic radiation. The maximum absorption in these materials coincides with the change from dielectric to metallic. The materials may be employed as antireflecting covering against ultraviolet rays because of the high reported peaks in the reflectivity $R(\omega)$ value. In contrast to $RbSnI_3$ and $CsSnI_3$, which have poor thermal conductivities, $KSnI_3$ has high thermal conductivity. Compared with $KSnI_3$ and $RbSnI_3$, $CsSnI_3$ has a substantially steeper thermal conductivity slope. The high electron energy in the $CsSnI_3$ material may be responsible for this. All three materials exhibit an increase in susceptibility from 100 to 800 K, which may be attributed to the temperature influence on electron spin mobility. The Seebeck coefficient reveals a p-type nature in the investigated material, and the positive R_H agrees with the electronic features.

AUTHOR INFORMATION

Corresponding Author

Muhammad Salman Khan − *Department of Physics, Abdul Wali Khan University, Mardan 23200, Pakistan;* orcid.org/0000-0001-9909-0883; Email: salmankhan73030@gmail.com

Authors

Banat Gul − *National University of Sciences and Technology (NUST), Islamabad 44000, Pakistan*

Muhammad Aasim − *Department of Physics, Abdul Wali Khan University, Mardan 23200, Pakistan*

Ahmad A. Ifseisi − *Department of Chemistry, College of Science, King Saud University, Riyadh 11451, Saudi Arabia*

Gulzar Khan − *Department of Physics, Abdul Wali Khan University, Mardan 23200, Pakistan*

Hijaz Ahmad − *Section of Mathematics, International Telematic University Uninettuno, 00186 Roma, Italy;* orcid.org/0000-0002-5438-5407

Complete contact information is available at: https://pubs.acs.org/10.1021/acsomega.3c03756

Notes

The authors declare no competing financial interest.

ACKNOWLEDGMENTS

The authors are grateful to the Researchers Supporting Project Number (RSPD2023R669), King Saud University, Riyadh, Saudi Arabia for the financial support.

REFERENCES

(1) Yang, W.; Noh, J.; Jeon, N.; Kim, Y.; Ryu, S.; Seo, J.; et al. High-performance photovoltaic perovskite layers fabricated through intramolecular exchange. *Science* **2015**, *348*, 1234−1237.

(2) Dong, R.; Fang, Y.; Chae, J.; Dai, J.; Xiao, Z.; Dong, Q.; et al. High-Gain and Low-Driving-Voltage Photodetectors Based on Organolead Triiodide Perovskites. *Adv. Mater.* **2015**, *27*, 1912−1918.

(3) Dou, L.; Yang, Y.; You, J.; Hong, Z.; Chang, W.; Li, G.; et al. Solution-processed hybrid perovskite photodetectors with high detectivity. *Nat. Commun.* **2014**, *5*, 5404.

(4) Edri, E.; Kirmayer, S.; Cahen, D.; Hodes, G. High Open-Circuit Voltage Solar Cells Based on Organic−Inorganic Lead Bromide Perovskite. *J. Phys. Chem. Lett.* **2013**, *4*, 897−902.

(5) Saidaminov, M.; Adinolfi, V.; Comin, R.; Abdelhady, A.; Peng, W.; Dursun, I.; et al. Planar-integrated single-crystalline perovskite photodetectors. *Nat. Commun.* **2015**, *6*, 8724.

(6) Salman Khan, M.; Gul, B.; Khan, G.; Benaadad, M.; Ghlamallah, B.; Ali Khattak, S.; Khan, T.; Zulfiqar, S.; Shah, S. K.; Adil Khan, M.; et al. Ab-initio study about the electronic, optical and thermoelectric nature of α-, β-, and γ-phases of CdS semiconductor: using the accurate m-BJ approach. *Phys. Scr.* **2021**, *96*, No. 055803.

(7) Afsari, M.; Boochani, A.; Hantezadeh, M. Electronic, optical and elastic properties of cubic perovskite CsPbI3: Using first principles study. *Optik* **2016**, *127*, 11433−11443.

(8) Sutherland, B.; Hoogland, S.; Adachi, M.; Wong, C.; Sargent, E. Conformal Organohalide Perovskites Enable Lasing on Spherical Resonators. *ACS Nano* **2014**, *8*, 10947−10952.

(9) Zhu, H.; Fu, Y.; Meng, F.; Wu, X.; Gong, Z.; Ding, Q.; et al. Lead halide perovskite nanowire lasers with low lasing thresholds and high-quality factors. *Nat. Mater.* **2015**, *14*, 636−642.

(10) Hayatullah; Murtaza, G.; Muhammad, S.; Naeem, S.; Khalid, M.; Manzar, A. Physical Properties of $CsSnM_3$ (M = Cl, Br, I): A First Principle Study. *Acta Phys. Polym., A* **2013**, *124*, 102−107.

(11) Babu, K. E.; Murali, N.; Babu, K. V.; Shibeshi, P. T.; Veeraiah, V. Structural, Elastic, Electronic, and Optical Properties of Cubic Perovskite CsCaCl3 Compound: An ab initio Study. *Acta Phys. Pol. A* **2014**, *125*, 1179−1185.

(12) Jishi, R. A. Modified Becke-Johnson exchange potential: improved modeling of lead halides for solar cell applications. *AIMS Mater. Sci.* **2016**, *3*, 149−159.

(13) Tran, F.; Blaha, P.; Schwarz, K. Band gap calculations with Becke−Johnson exchange potential. *J. Phys.: Condens. Matter* **2007**, *19*, No. 196208.

(14) Kumar, I.; Song, J.; Im, J.; Androulakis, J.; Malliakas, C.; Li, H.; et al. CsSnI3: Semiconductor or Metal? High Electrical Conductivity and Strong Near-Infrared Photoluminescence from a Single Material. High Hole Mobility and Phase-Transitions. *J. Am. Chem. Soc.* **2012**, *134*, 8579−8587.

(15) Chung, I.; Lee, B.; He, J.; Chang, R.; Kanatzidis, M. All-solid-state dye-sensitized solar cells with high efficiency. *Nature* **2012**, *485*, 486−489.

(16) Ogomi, Y.; Morita, A.; Tsukamoto, S.; Saitho, T.; Fujikawa, N.; Shen, Q.; et al. $CH_3NH_3Sn_xPb_{(1-x)}I_3$ Perovskite Solar Cells Covering up to 1060 nm. *J. Phys. Chem. Lett.* **2014**, *5*, 1004−1011.
(17) Petrović, M.; Chellappan, V.; Ramakrishna, S. Perovskites: Solar cells & engineering applications − materials and device developments. *Sol. Energy* **2015**, *122*, 678−699.
(18) Saliba, M.; Matsui, T.; Seo, J.; Domanski, K.; Correa-Baena, J.; Nazeeruddin, M.; et al. Cesium-containing triple cation perovskite solar cells: improved stability, reproducibility and high efficiency. *Energy Environ. Sci.* **2016**, *9*, 1989−1997.
(19) Saliba, M.; Matsui, T.; Domanski, K.; Seo, J.; Ummadisingu, A.; Zakeeruddin, S.; et al. Incorporation of rubidium cations into perovskite solar cells improves photovoltaic performance. *Science* **2016**, *354*, 206−209.
(20) Ilvonen, O. Assessing release of hazardous substances from construction products − Review of 10 years of experience with a horizontal approach in the European Union. *Build. Environ.* **2013**, *69*, 194−205.
(21) Schwarz, K.; Blaha, P.; Madsen, G. Electronic structure calculations of solids using the Wien2k package for material sciences. *Comput. Phys. Commun.* **2002**, *147*, 71−76.
(22) Tran, F.; Blaha, P. Accurate Band Gaps of Semiconductors and Insulators with a Semilocal Exchange-Correlation Potential. *Phys. Rev. Lett.* **2009**, *102*, No. 226401.
(23) Perdew, J. P.; Zunger, A. Self-interaction correction to density-functional approximations for many-electron systems. *Phys. Rev. B* **1981**, *23*, 5048.
(24) Perdew, J.; Burke, K.; Ernzerhof, M. Generalized Gradient Approximation Made Simple. *Phys. Rev. Lett.* **1996**, *77*, 3865−3868.
(25) Khan, M. S.; Alshahrani, T.; Haq, B. U.; Azam, S.; Khan, G.; Alrobei, H.; Abbas, Z.; Předota, M.; Khan, M. A.; Benaadad, M.; et al. Investigation of structural, electronic and optical properties of potassium and lithium based ternary Selenoindate: Using first principles approach. *J. Solid State Chem.* **2021**, *293*, No. 121778.
(26) Aggarwal, K. Comment on "Relativistic atomic data for W XLVII" by S. Aggarwal et al. *Chin. Phys. B* **2015**, *24*, No. 123201.
(27) Burgelman, M.; Nollet, P.; Degrave, S. Modelling polycrystalline semiconductor solar cells. *Thin Solid Films* **2000**, *361*, 527−532.
(28) Khan, M. S.; Gul, B.; Khan, G.; Ghlamallah, B.; Khattak, S.; Khan, M.; et al. Insight into the electronic, optical and transport nature of Al_2CdX_4 (X = S, Se and Te) employing the accurate mBJ approach: Novel materials for opto-electronic devices. *Mater. Sci. Semicond. Process* **2021**, *135*, No. 106098.
(29) Qiu, X.; Cao, B.; Yuan, S.; Chen, X.; Qiu, Z.; Jiang, Y.; et al. From unstable $CsSnI_3$ to air-stable Cs_2SnI_6: A lead-free perovskite solar cell light absorber with bandgap of 1.48 eV and high absorption coefficient. *Sol. Energy Mater. Sol. Cells* **2017**, *159*, 227−234.
(30) Swarnkar, A.; Marshall, A.; Sanehira, E.; Chernomordik, B.; Moore, D.; Christians, J.; et al. Quantum dot−induced phase stabilization of α-$CsPbI_3$ perovskite for high-efficiency photovoltaics. *Science* **2016**, *354*, 92−95.
(31) Zeng, Q.; Zhang, X.; Liu, C.; Feng, T.; Chen, Z.; Zhang, W.; et al. Inorganic CsPbI2Br Perovskite Solar Cells: The Progress and Perspective. *Sol. RRL* **2019**, *3*, No. 1800239.
(32) Wang, G.; Liu, J.; Chen, K.; Pathak, R.; Gurung, A.; Qiao, Q. High-performance carbon electrode-based $CsPbI_2Br$ inorganic perovskite solar cell based on poly(3-hexylthiophene)-carbon nanotubes composite hole-transporting layer. *J. Colloid Interface Sci.* **2019**, *555*, 180−186.
(33) Nyayban, A.; Panda, S.; Chowdhury, A. Structural, electronic and optical properties of lead free Rb based triiodide for photovoltaic application: an ab initio study. *J. Phys.: Condens. Matter* **2021**, *33*, 375702.
(34) Thiele, G.; Serr, B. Crystal structure of rubidium triiodostannate (II), $RbSnI_3$. *Z. Kristallogr. - Cryst. Mater.* **1995**, *210*, 64.
(35) Kar, M.; Körzdörfer, T. Computational high throughput screening of inorganic cation based halide perovskites for perovskite only tandem solar cells. *Mater. Res. Express* **2020**, *7*, No. 055502.
(36) Tao, S.; Cao, X.; Bobbert, P. Accurate and Efficient Band Gap Predictions of Metal Halide Perovskites Using the DFT-1/2 Method: GW Accuracy with DFT Expense. *Sci. Rep.* **2017**, *7*, 14386.
(37) Lang, L.; Zhang, Y.; Xu, P.; Chen, S.; Xiang, H.; Gong, X. Three-Step Approach for Computing Band Offsets and Its Application to Inorganic ABX_3 Halide Perovskites. *Phys. Rev. B* **2015**, *92*, No. 075102.
(38) Jiang, J.; Onwudinanti, C.; Hatton, R.; Bobbert, P.; Tao, S. Stabilizing Lead-Free All-Inorganic Tin Halide Perovskites by Ion Exchange. *J. Phys. Chem. C* **2018**, *122*, 17660−17667.
(39) Lee, M. M.; Teuscher, J.; Miyasaka, T.; Murakami, T. N.; Snaith, H. J. Efficient Hybrid Solar Cells Based on Meso-Superstructured Organometal Halide Perovskites. *Science* **2012**, *338*, 643.
(40) King-Smith, R. D.; Vanderbilt, D. First-principles investigation of ferroelectricity in perovskite compounds. *Phys. Rev. B* **1994**, *49*, 5828.
(41) Huang, L.-y.; Lambrecht, W. R. L. *Phys. Rev. B* **2014**, *90*, No. 195201.
(42) Penn, D. R. Wave-number-dependent dielectric function of semiconductors. *Phys. Rev.* **1962**, *128*, 2093.
(43) Khan, M. S.; Gul, B.; Abu-Farsakh, H.; Khan, G. Insight into the Optoelectronic and Thermoelectric Nature of NaLiX (X = S, Se, Te) Novel Direct Bandgap Semiconductors: A First-Principles Study. *J. Mater. Chem. C* **2022**, *10*, 12001−12011.
(44) MØLLER, CHR. KN. Crystal Structure and Photoconductivity of Cæsium Plumbohalides. *Nature* **1958**, *182*, 1436−1436.

https://doi.org/10.1021/acsomega.3c03756
ACS Omega 2023, 8, 32784−32793